JACS
JOURNAL OF THE AMERICAN CHEMICAL SOCIETY

Communication

pubs.acs.org/JACS

Dopant-Free Hole-Transporting Material with a C_{3h} Symmetrical Truxene Core for Highly Efficient Perovskite Solar Cells

Chuyi Huang,[†,∥] Weifei Fu,[†,∥] Chang-Zhi Li,[*,†] Zhongqiang Zhang,[†] Weiming Qiu,[‡] Minmin Shi,[†] Paul Heremans,[‡] Alex K.-Y. Jen,[*,†,§] and Hongzheng Chen[*,†]

[†]MOE Key Laboratory of Macromolecular Synthesis and Functionalization, State Key Laboratory of Silicon Materials, Department of Polymer Science and Engineering, Zhejiang University, Hangzhou 310027, P. R. China

[‡]Imec, Kapeldreef 75, 3001 Heverlee, Belgium

[§]Department of Materials Science & Engineering, University of Washington, Seattle, Washington 98195, United States

Supporting Information

ABSTRACT: Herein we present a new structural design of hole-transporting material, Trux-OMeTAD, which consists of a C_{3h} Truxene-core with arylamine terminals and hexyl side-chains. This planar, rigid, and fully conjugated molecule exhibits excellent hole mobility and desired surface energy to the perovskite uplayer. Perovskite solar cells fabricated using the p-i-n architecture with Trux-OMeTAD as the p-layer, show a high PCE of 18.6% with minimal hysteresis.

Perovskite solar cells (PVSCs) made with ammonium lead halide,[1] such as $CH_3NH_3PbI_3$ have recently gained significant attention due to their capabilities in achieving high power conversion efficiency (PCE) through cost-effective fabrication.[1−4] The PCE of PVSC has shown exceptionally fast growth rising from 3.8% to 20.1% within only six years.[1,5−9] In the well-performing PVSCs, charge-transporting layers consist of organic/inorganic electron (ETM) and hole (HTM) transporting materials are needed in order to facilitate the free carrier collection to the corresponding electrodes.[10−21] Although significant development of PVSC has been achieved, this is accomplished through very limited number of good HTMs, such as the frequently used poly(3,4-ethylenedioxythiophene) polystyrenesulfonate (PEDOT:PSS), arylamine based derivatives, 2,2′,7,7′-tetrakis(*N*,*N*-di-*p*-methoxyphenylamine)-9,9′-spirobifluorene (Spiro-OMeTAD), and polytriarylamine (PTAA). In addition to the limited HTM availability, there are also several obstacles that need to be overcome in order to facilitate the further development of versatile and efficient PVSCs, such as the complicated doping protocol, mismatched energy levels, relatively high cost, and limited long-term stability.

In this regard, it is highly desirable to develop new HTM for further improving PVSC device efficiency and stability and probing their structure−property correlations. There are several factors beyond mobility and energy level that need to be considered when design new HTMs. Recent reports revealed that hydrophobic surface,[22] perovskite surface passivation,[23] and even UV light cutoff can all be engineered as part of HTM properties to either facilitate the growth of large crystal grain or prevent UV light induced perovskite degradation.[24] However, it is a significant challenge to integrate all these desirable features into a single HTM.

In this study, we present a new design of HTM that promotes excellent contact between perovskite and the underneath transparent electrode. The new HTM, Trux-OMeTAD, consists of a C_{3h} Truxene-core with three arylamine groups, and six hexyl side-chains, adapting a planar, rigid, and fully conjugated molecular geometry. These features enable Trux-OMeTAD to have high hole mobility, suitable surface energy, and matched frontier energy level with the top perovskite layer. As a result, PVSCs fabricated with the p-i-n architecture using Trux-OMeTAD as the p-layer show a high PCE of 18.6% with minimal hysteresis under AM 1.5 G illumination, which is one of the highest values reported so far for the p-i-n PVSC devices employing dopant-free HTMs.

The synthetic routes for making Trux-OMeTAD are shown in Figure 1a, with details described in the Supporting Information (SI). The Truxene unit was first synthesized through the condensation of 1-indanone.[25] The *para*-methoxy diphenylamine was then introduced by the Buchwald−Hartwig amination reaction, resulting in Trux-OMeTAD in 70% yield (Figure S1).

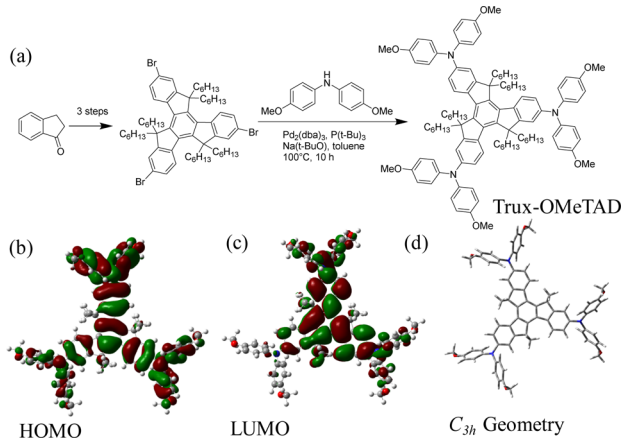

Figure 1. (a) Four-steps synthetic routes for Trux-OMeTAD. (b) HOMO, (c) LUMO, and (d) optimized molecular conformation obtained from DFT calculations.

Received: January 4, 2016
Published: February 15, 2016

DOI: 10.1021/jacs.6b00039
J. Am. Chem. Soc. 2016, 138, 2528−2531

The pale yellow final product was characterized by ^{1}H and ^{13}C NMR spectra and MALDI-TOF mass spectrometry (Figures S2–S4). Thermal properties of Trux-OMeTAD were tested via thermogravimetric analysis (TGA) and differential scanning calorimetry (DSC) (Figures S5 and S6). The TGA curves indicated that Trux-OMeTAD is thermally stable up to 400 °C. The melting peak at 212 °C appeared on the DSC curve indicates this material is crystalline in solid-state. This coincides well with the observation of polarized optical microscopy (POM) showing the formation of needle-like crystals during drying of the saturated Trux-OMeTAD hexane solution on glass slides (Figure S7). Note that the Truxene is a typical discotic mesogen,[26] which tends to form face-on packed molecular assemblies with a columnar arrangement.[27] This is one of the ideal superstructures for π-conjugated molecules to facilitate vertical hole transport.

To gain further understanding on its electronic structure, the molecular orbitals (MO) of Trux-OMeTAD were calculated through the density functional theory (DFT) (SI). As shown in Figure 1b–d, both the highest occupied and the lowest unoccupied MOs, HOMO and LUMO, respectively show that the electron density of Trux-OMeTAD is fully delocalized within the whole molecule. The methoxy group bearing oxygen lone-pair points out-of-plane. Note that the Lewis basic heteroatom, can potentially passivate perovskite surface, i.e., by coordinating with lead ion via halide vacancies.[18,23,28,29] In addition, the planar, rigid, and fully conjugated molecule with the C_{3h} geometry enables Trux-OMeTAD to have ordered assemblies for better charge transport in film state.

Figure 2a shows the UV–vis absorption and transmittance of Trux-OMeTAD film, displaying an absorption edge at 410 nm,

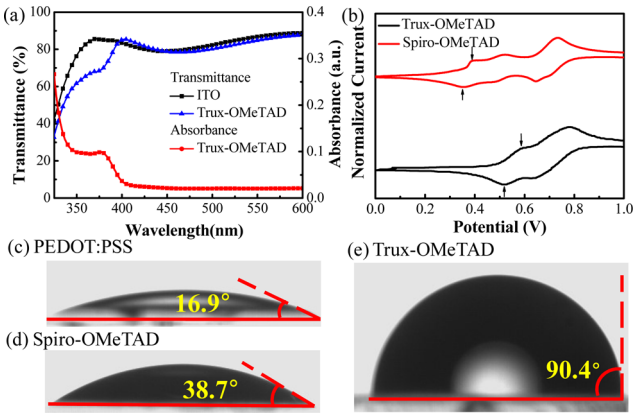

Figure 2. (a) UV–vis transmittance and absorbance of Trux-OMeTAD film (15 nm). (b) Cyclic voltammograms of Trux-OMeTAD and Spiro-OMeTAD. Water contact angles on (c) PEDOT:PSS, (d) as-cast Spiro-OMeTAD, and (e) Trux-OMeTAD films.

which is corresponding to an optical bandgap of 3.02 eV. It is nearly transparent in the region between visible and near-infrared region. These are the desired optical properties for a HTM layer in perovskite-based solar cells. Additionally, we observed a slightly red-shifted absorption peak together with a shoulder peak appeared upon thermal annealing of Trux-OMeTAD film (Figure S8), suggesting the possible thermotropic alignment of molecules. More interestingly, the absorption of Trux-OMeTAD layer can reduce UV light that is known to cause light-induced perovskite degradation.[30] To probe these relative energy levels between Trux-OMeTAD and Spiro-OMeTAD, cyclic voltammetry was employed to compare the redox properties (Figure 2b). The results indicate that the HOMO energy level of Trux-OMeTAD (−5.28 eV) is 0.18 eV deeper than that of Spiro-OMeTAD (−5.10 eV), which is better matched with the valence band of $CH_3NH_3PbI_3$ perovskite (−5.4 eV).

In addition to frontier energetics, surface wettability of the bottom charge-transporting layer is also an important factor that significantly affects the morphology of perovskite films. Recent reports suggested that a relatively hydrophobic surface will facilitate the formation of good quality perovskite polycrystalline films, comparing with those fabricated atop of a hydrophilic surface.[22] In Trux-OMeTAD, in addition to its aromatic Truxene plane, six aliphatic chains were introduced. The nonpolar, flexible chains can modulate the HTM surface energy, i.e., staying at the solid/gas interface. This is quite different from those of Spiro-OMeTAD and PTAA, bearing no aliphatic chains. The contact angle tests showed that PEDOT:PSS, as expected, exhibits a smaller contact angle (16.9°) to water droplet (Figure 2c). The as-cast Spiro-OMeTAD exhibits a contact angle of 38.7°. As a sharp contrast, the Trux-OMeTAD exhibits a much larger contact angle of 90.4° (the film was annealed at 150 °C for 10 min) (Figure 2d,e). The surface morphology of HTMs layers was measured by tapping mode atomic force microscopy (AFM) (Figure S9), showing a smooth surface with a root-mean-square (RMS) roughness of 2.4 nm. Such hydrophobic and smooth HTM layer should be beneficial for achieving high-quality perovskite films.

Prior to solar cell fabrication, the hole-transport of Trux-OMeTAD was measured by using the space-charge-limited-current (SCLC) technique (Figures S10 and S11). To verify the effect of film annealing on the correspondent hole-transport, the HTM film was annealed at different temperatures. The as-cast Trux-OMeTAD film exhibits a hole mobility of 2.3×10^{-3} $cm^2 \cdot V^{-1} \cdot s^{-1}$, and increases to 3.6×10^{-3} $cm^2 \cdot V^{-1} \cdot s^{-1}$ after being annealed at 150 °C for 10 min. This is nearly 2 orders of magnitude higher than those of neat Spiro-OMeTAD and PTAA (between 10^{-5} and 10^{-4} $cm^2 \cdot V^{-1} \cdot s^{-1}$, Table S1).[31] The high mobility allows it to function as an effective HTM without the need of extra doping process, which significantly simplifies device fabrication.

With these data in hand, the p-i-n structure PVSCs was fabricated (Figure 3a) to elucidate the structural–property correlations of Trux-OMeTAD as a p-layer for hole extraction. The device was made by fabricating of a layer of $CH_3NH_3PbI_3$ (~300 nm) atop of Trux-OMeTAD (~15 nm) using the two-step deposition method (SI). The ETM layer employs a bilayer of PCBM (~40 nm) and ZnO nanoparticles (~40 nm), and Al (~100 nm) was used as cathode. The energy diagram of each layer is shown in Figure 3b. It displays better matched HOMO levels between Trux-OMeTAD and perovskite that not only facilitate efficient hole transfer and extraction but also decrease energy loss in between. The high LUMO (−2.3 eV) of Trux-OMeTAD can also effectively block electrons to prevent recombination at anode. The devices were optimized by annealing the Trux-OMeTAD layer at different temperatures and thickness without applying any dopants or additives (Figures S12 and S13). The performance showed negligible sensitivity toward the varied thickness in the range of 2–30 nm. The best device was achieved with the HTL annealed at 150 °C for 10 min (Table S2).

Figure 3c shows the current density–voltage (J–V) curves for the best device under the standard AM 1.5G illumination. The results are summarized in Table 1. The best device yields a high PCE of 18.6% with an open circuit voltage (V_{OC}) of 1.02 V, a

DOI: 10.1021/jacs.6b00039
J. Am. Chem. Soc. 2016, 138, 2528–2531

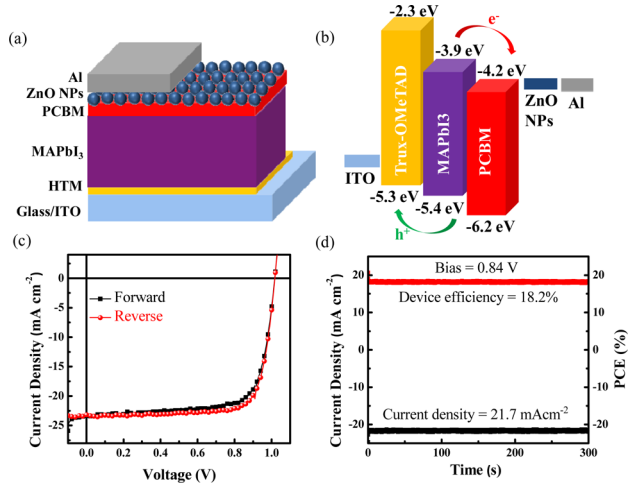

Figure 3. (a) Schematic of the planar p-i-n PVSC with Trux-OMeTAD HTM. (b) Energy level diagram for each layer of the PVSC device. (c) *J*–*V* curves of the device with 150 °C annealed HTM. (d) Stabilized photocurrent measurement of the best device and its power output.

Table 1. Current Density–Voltage (*J*–*V*) Curves of PVSCs Using Trux-OMeTAD HTM under AM 1.5G Illumination (100 mW·cm^{-2})

devices	V_{OC} [V]	J_{SC} [mA·cm^{-2}]	FF	PCE [%]
forward scan	1.02	23.4	0.74	17.5
reverse scan	1.02	23.2	0.79	18.6

short circuit current density (J_{SC}) of 23.2 mA·cm^{-2}, and a fill factor (FF) of 0.79, by sweeping from forward bias (1.2 V) to reverse bias (−0.1 V). In the reverse scan from reverse bias (−0.1 V) to forward bias (1.2 V), a PCE of 17.5% can be retained with a V_{OC} of 1.02 V, a J_{SC} of 23.4 mA·cm^{-2}, and a FF of 0.74. No apparent hysteresis could be detected during forward and reverse scans. The external quantum efficiency (EQE) spectrum of the perovskite solar cell is shown in Figure S14, which is consistent with measured *J*sc. The PCE of 18.6% is one of the highest values among the p-i-n PVSC devices employing dopant-free HTMs up to date. The widely used HTMs, such as PEDOT:PSS, PTAA, and Spiro-OMeTAD were tested using the same device architecture showing the PCEs of around 16%, which are clearly lower than that obtained for Trux-OMeTAD based devices. HTM-free device was also fabricated that showed much lower PCE of 8.61% than those devices with HTM layer (Figure S15, Table S3). To confirm our results, the photocurrent density and PCE as a function of time at the maximum power point (0.84 V) were measured. As shown in Figure 3d, the photocurrent and PCE remained stable toward 300 s scan, and a stable PCE output over 18% was demonstrated.

Good reproducibility is also demonstrated for PVSCs using this dopant-free HTM. The efficiency histogram in Figure 4 shows >75% of the devices (among 30 devices) having PCE higher than 17%. To further understand the effects of Trux-OMeTAD HTM on perovskite uplayer, steady-state PL and time-resolved PL decay measurements were conducted for neat perovskite film, perovskite with nonannealed HTM, and perovskite with 150 °C annealed HTM. The surface and cross-sectional morphology of the perovskite films fabricated atop of HTM layer are also characterized by scanning electron microscopy (SEM).

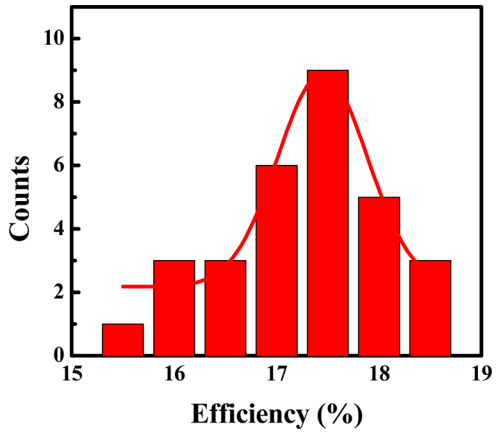

Figure 4. Histograms of 30 device PCEs based on 150 °C annealed Trux-OMeTAD HTM.

Figure 5a shows the PL spectra of perovskite on different substrates. The enhanced PL quenching of perovskite was

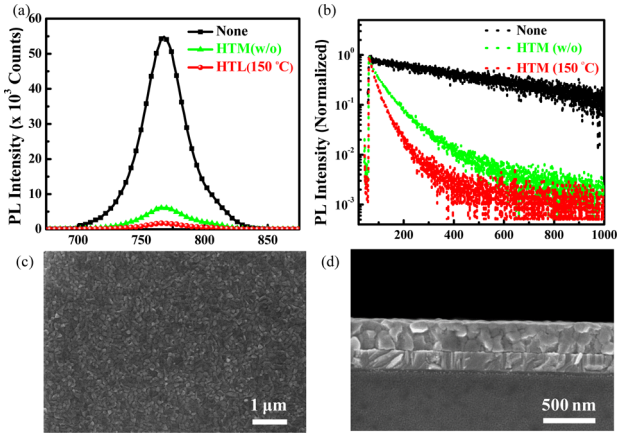

Figure 5. (a) Steady state photoluminescence (PL) spectra of the perovskite films on different substrates (glass only, glass/nonannealed HTM, and glass/annealed HTM). (b) Time-resolved PL measurements taken at the peak emission wavelength (765 nm) of the perovskite films on different substrates. A 5 mW picosecond pulsed diode laser at 638.8 nm excited on the glass side. (c) Top view and (d) cross-sectional SEM images of the perovskite film atop of annealed HTM layer.

observed for the substrate using 150 °C annealed HTM compared to those without annealing. This suggests that carriers created in the excited perovskite layers are more efficiently extracted by the annealed HTM, which coincides well with the improved SCLC hole mobility observed in the annealed HTM. The steady state PL spectra of perovskite on PEDOT:PSS showed in Figure S16, which indicate PEDOT:PSS is less effective in quenching the excited perovskite than that of Trux-OMeTAD. In order to verify the improved hole transfer, the time-resolved PL measurements were conducted and shown in Figure 5b, and the results were summarized in Table 2. The

Table 2. Time-Resolved PL Measurements

sample	τ_1 (ns)	frac. 1	τ_2 (ns)	frac. 2	ave. (ns)
none	108.0	1.9%	1004.8	98.1%	987.8
HTM (w/o)	32.0	40.6%	107.1	59.4%	76.6
HTM (150 °C)	21.0	60.8%	67.6	39.2%	39.1

DOI: 10.1021/jacs.6b00039
J. Am. Chem. Soc. 2016, 138, 2528–2531

perovskite-only film exhibits an averaged decay time (ave. τ) of 987.8 ns. After the introduction of Trux-OMeTAD beneath the perovskite, the averaged τ is shortened to 76.6 ns (without annealing) and 39.1 ns (with 150 °C annealing). The fast decay lifetime τ_1 of three samples decreased from 108 ns (neat perovskite) to 32.0 ns (nonannealed HTM) and 21.0 ns (150 °C annealed HTM), while the weight fraction increased from 1.9% to 40.6% (without annealing) and 60.8% (with annealing). This indicates improved hole extraction and charge dissociation from perovskite to the treated HTM.

Figure 5c illustrated the perovskite film fabricated atop of the annealed HTM layer, showing a smooth and dense perovskite film. The cross-sectional SEM images (Figure 5d) showed ordered and vertically aligned grain boundaries, which should be beneficial for the infiltration of transporting materials to suppress recombination loss and enhance carrier collection.[32] As comparison, the perovskite film atop of Trux-OMeTAD exhibited slightly larger and denser grains than those on PEDOT:PSS (Figure S17). The PL and morphology results correlate well with the increased HTM hole mobility, and the significantly enhanced PVSC performance on annealed HTM layer.

In summary, a novel HTM was developed by introducing triarylamine and aliphatic side-chains onto the C_{3h} Truxene-core to successfully demonstrate its application for highly efficient and stable PVSCs. A PCE as high as 18.6% was achieved from devices fabricated through a simple solution process. The planar and fully conjugated C_{3h} HTM result in excellent hole mobility and proper surface energy for the perovskite layer cast atop to facilitate more efficient hole extraction for achieving high-performance PVSCs.

■ ASSOCIATED CONTENT

Supporting Information

The Supporting Information is available free of charge on the ACS Publications website at DOI: 10.1021/jacs.6b00039.

Experimental details for the synthesis and supplementary figures (PDF)

■ AUTHOR INFORMATION

Corresponding Authors

*czli@zju.edu.cn
*ajen@u.washington.edu
*hzchen@zju.edu.cn

Author Contributions

‖C.H. and W.F. contributed equally in this work.

Notes

The authors declare no competing financial interest.

■ ACKNOWLEDGMENTS

The authors thank the financial support from the National Natural Science Foundation of China (No. 51473142). The study was also partly supported by 973 program (No. 2014CB643503). C.-Z.L. thanks the financial support from the National 1000 Young Talents Program by China government, and 100 Talents Program by Zhejiang University. A.K.-Y.J. thanks the Boeing-Johnson Foundation for its support.

■ REFERENCES

(1) Kojima, A.; Teshima, K.; Shirai, Y.; Miyasaka, T. *J. Am. Chem. Soc.* **2009**, *131*, 6050.
(2) Nazeeruddin, M. K.; Snaith, H. *MRS Bull.* **2015**, *40*, 641.
(3) Sessolo, M.; Bolink, H. J. *Nat. Mater.* **2015**, *14*, 964.
(4) Green, M. A.; Ho-Baillie, A.; Snaith, H. J. *Nat. Photonics* **2014**, *8*, 506.
(5) Zhou, H.; Chen, Q.; Li, G.; Luo, S.; Song, T.-b.; Duan, H.-S.; Hong, Z.; You, J.; Liu, Y.; Yang, Y. *Science* **2014**, *345*, 542.
(6) Snaith, H. J. *J. Phys. Chem. Lett.* **2013**, *4*, 3623.
(7) Park, N.-G. *J. Phys. Chem. Lett.* **2013**, *4*, 2423.
(8) Yang, W. S.; Noh, J. H.; Jeon, N. J.; Kim, Y. C.; Ryu, S.; Seo, J.; Seok, S. I. *Science* **2015**, *348*, 1234.
(9) Li, W. Z.; Fan, J. D.; Li, J. W.; Mai, Y. H.; Wang, L. D. *J. Am. Chem. Soc.* **2015**, *137*, 10399.
(10) Wang, Q.; Shao, Y.; Dong, Q.; Xiao, Z.; Yuan, Y.; Huang, J. *Energy Environ. Sci.* **2014**, *7*, 2359.
(11) Liang, P.-W.; Liao, C.-Y.; Chueh, C.-C.; Zuo, F.; Williams, S. T.; Xin, X.-K.; Lin, J.; Jen, A. K. Y. *Adv. Mater.* **2014**, *26*, 3748.
(12) Ball, J. M.; Lee, M. M.; Hey, A.; Snaith, H. J. *Energy Environ. Sci.* **2013**, *6*, 1739.
(13) Malinkiewicz, O.; Yella, A.; Lee, Y. H.; Espallargas, G. M.; Graetzel, M.; Nazeeruddin, M. K.; Bolink, H. J. *Nat. Photonics* **2014**, *8*, 128.
(14) Lin, Q.; Armin, A.; Nagiri, R. C. R.; Burn, P. L.; Meredith, P. *Nat. Photonics* **2015**, *9*, 106−112.
(15) Guo, Y.; Liu, C.; Inoue, K.; Harano, K.; Tanaka, H.; Nakamura, E. *J. Mater. Chem. A* **2014**, *2*, 13827.
(16) Malinkiewicz, O.; Roldán-Carmona, C.; Soriano, A.; Bandiello, E.; Camacho, L.; Nazeeruddin, M. K.; Bolink, H. J. *Adv. Energy Mater.* **2014**, *4*, 1400345.
(17) Kim, H.; Lim, K.-G.; Lee, T.-W. *Energy Environ. Sci.* **2016**, *12*, 12−30.
(18) Cao, J.; Liu, Y. M.; Jing, X.; Yin, J.; Li, J.; Xu, B.; Tan, Y. Z.; Zheng, N. *J. Am. Chem. Soc.* **2015**, *137*, 10914.
(19) Li, Y.; Zhao, Y.; Chen, Q.; Yang, Y. M.; Liu, Y.; Hong, Z.; Liu, Z.; Hsieh, Y. T.; Meng, L.; Li, Y.; Yang, Y. *J. Am. Chem. Soc.* **2015**, *137*, 15540.
(20) Li, C. Z.; Liang, P. W.; Sulas, D. B.; Nguyen, P. D.; Li, X. S.; Ginger, D. S.; Schlenker, C. W.; Jen, A. K. Y. *Mater. Horiz.* **2015**, *2*, 414.
(21) Zuo, L. J.; Gu, Z. W.; Ye, T.; Fu, W. F.; Wu, G.; Li, H. Y.; Chen, H. Z. *J. Am. Chem. Soc.* **2015**, *137*, 2674.
(22) Bi, C.; Wang, Q.; Shao, Y.; Yuan, Y.; Xiao, Z.; Huang, J. *Nat. Commun.* **2015**, *6*, 7747.
(23) deQuilettes, D. W.; Vorpahl, S. M.; Stranks, S. D.; Nagaoka, H.; Eperon, G. E.; Ziffer, M. E.; Snaith, H. J.; Ginger, D. S. *Science* **2015**, *348*, 683.
(24) Berhe, T. A.; Su, W.-N.; Chen, C.-H.; Pan, C.-J.; Cheng, J.-H.; Chen, H.-M.; Tsai, M.-C.; Chen, L.-Y.; Dubale, A. A.; Hwang, B.-J. *Energy Environ. Sci.* **2016**, *9*, 323.
(25) Cao, X. Y.; Zhou, X. H.; Zi, H.; Pei, J. *Macromolecules* **2004**, *37*, 8874.
(26) Goodby, J.; P. J. C, Kato, T.; Tschierske, C.; Gleeson, H.; Raynes, P., Eds. *Handbook of Liquid Crystals*; Wiley-VCH: Weinheim, 1998; p 693.
(27) Ni, H.-L.; Monobe, H.; Hu, P.; Wang, B.-Q.; Shimizu, Y.; Zhao, K.-Q. *Liq. Cryst.* **2013**, *40*, 411.
(28) Sun, C.; Wu, Z.; Yip, H.-L.; Zhang, H.; Jiang, X.-F.; Xue, Q.; Hu, Z.; Hu, Z.; Shen, Y.; Wang, M.; Huang, F.; Cao, Y. *Adv. Energy Mater.* **2015**, 1534.
(29) Kim, Y. H.; Cho, H.; Heo, J. H.; Kim, T. S.; Myoung, N.; Lee, C. L.; Im, S. H.; Lee, T. W. *Adv. Mater.* **2015**, *27*, 1248.
(30) Ahmad, S.; Kanaujia, P. K.; Niu, W.; Baumberg, J. J.; Prakash, G. V. *ACS Appl. Mater. Interfaces* **2014**, *6*, 10238.
(31) Poplavskyy, D.; Nelson, J. *J. Appl. Phys.* **2003**, *93*, 341.
(32) Yang, B.; Dyck, O.; Poplawsky, J.; Keum, J.; Puretzky, A.; Das, S.; Ivanov, I.; Rouleau, C.; Duscher, G.; Geohegan, D.; Xiao, K. *J. Am. Chem. Soc.* **2015**, *137*, 9210.

DOI: 10.1021/jacs.6b00039
J. Am. Chem. Soc. 2016, 138, 2528−2531